Seipin performs dissectible functions in promoting lipid droplet biogenesis and regulating droplet morphology

Bethany R. Cartwright, Derk D. Binns, Christopher L. Hilton, Sungwon Han, Qiang Gao, and Joel M. Goodman
Department of Pharmacology, University of Texas Southwestern Medical Center, Dallas, TX 75235-9041

ABSTRACT Seipin is necessary for both adipogenesis and lipid droplet (LD) organization in nonadipose tissues; however, its molecular function is incompletely understood. Phenotypes in the seipin-null mutant of *Saccharomyces cerevisiae* include aberrant droplet morphology (endoplasmic reticulum–droplet clusters and size heterogeneity) and sensitivity of droplet size to changes in phospholipid synthesis. It has not been clear, however, whether seipin acts in initiation of droplet synthesis or at a later step. Here we utilize a system of de novo droplet formation to show that the absence of seipin results in a delay in droplet appearance with concomitant accumulation of neutral lipid in membranes. We also demonstrate that seipin is required for vectorial budding of droplets toward the cytoplasm. Furthermore, we find that the normal rate of droplet initiation depends on 14 amino acids at the amino terminus of seipin, deletion of which results in fewer, larger droplets that are consistent with a delay in initiation but are otherwise normal in morphology. Importantly, other functions of seipin, namely vectorial budding and resistance to inositol, are retained in this mutant. We conclude that seipin has dissectible roles in both promoting early LD initiation and in regulating LD morphology, supporting its importance in LD biogenesis.

INTRODUCTION

Storage of energy is a universal and essential function of life. Storage of fat, or neutral lipids (NLs), is a primary function of mammalian adipocytes and plant oil seeds but also occurs in nearly every eukaryotic cell and even in some bacteria (Low *et al.*, 2010; Napier and Graham, 2010; Fujimoto and Parton, 2011; Kuhnlein, 2011; Mak, 2012; Yang *et al.*, 2012). Within the cell, fat is stored in cytoplasmic lipid droplets (LDs), particles derived from the endoplasmic reticulum (ER) that consist of a core of NLs surrounded by a phospholipid (PL) monolayer. The LD surface also contains a protein complement rich in lipid synthetic and modifying enzymes as well as proteins that modulate lipolysis, mediate protein and lipid trafficking, and facilitate interactions with other organelles, including other droplets (Binns *et al.*, 2006; Goodman, 2008, 2009; Gong *et al.*, 2011; Granneman *et al.*, 2011; Yang *et al.*, 2012). Once thought to be little more than passive storage depots or subcompartments of the ER, the unique protein and PL composition and the increasingly complex interactions described at the LD have led to a unified view of the LD as a dynamic organelle in its own right (Martin and Parton, 2006; Le Lay and Dugail, 2009).

The mechanism of LD biogenesis from the ER has stirred much interest but remains largely elusive. In the most widely accepted model, NL is believed to accumulate at its site of synthesis within the ER bilayer, coalescing into a "lens" or "blister" that then buds outward into the cytosol, very commonly with maintained connections to the ER (Martin and Parton, 2006; Adeyo *et al.*, 2011; Jacquier *et al.*, 2011; Wilfling *et al.*, 2013). While there is evidence for the involvement of proteins such as Fit2 or perilipin 3 in early steps of droplet biogenesis (Skinner *et al.*, 2009; Gross *et al.*, 2011), no factor

has yet been found to be essential for NL coalescence within the cell. Some groups have suggested that LDs are generated by spontaneous emulsion in processes driven by the physicochemical properties of NL and PL in an aqueous environment (Zanghellini et al., 2010; Thiam et al., 2013; Wilfling et al., 2014). However, it remains possible that cellular protein machinery may act to facilitate formation of the emulsion of NL into droplets (Wilfling et al., 2014).

One of the primary functions of the LD and of adipose tissue is to protect the rest of the organism from lipotoxicity. The importance of this function is made apparent by the metabolic consequences of disorders of fat storage in humans. While the saturation of lipid stores in obesity is a strong risk factor for metabolic imbalances and cardiovascular disease, disease at the other end of the spectrum—the absence of normal adipose tissue in lipodystrophy—can be even more devastating. Lipodystrophic patients suffer from several metabolic defects, including insulin-resistant diabetes and fatty liver (Garg, 2004; Agarwal and Garg, 2006). Congenital generalized lipodystrophy is attributed to loss-of-function mutations in cavin, caveolin, acyl-glycerol-phosphate acyltransferase 2, and, in the most severe cases, seipin (Garg, 2004; Cartwright and Goodman, 2012).

The importance of seipin in adipocyte function appears to be conserved in animals, as seipin knockouts in *Drosophila* and mice have also produced lipodystrophy, albeit not as severe as in humans (Cui et al., 2011; Tian et al., 2011; Chen et al., 2012; Prieur et al., 2013). Work in adipogenic cell culture models has indicated that the lipodystrophic phenotype is likely to result from a defect in adipocyte differentiation, although the etiology of this effect has yet to be conclusively determined (Payne et al., 2008; Chen et al., 2009, 2012; Prieur et al., 2013). Interestingly, several lines of evidence have indicated that seipin may exert distinct functions in adipose versus nonadipose cells, and two studies have found evolutionarily recent or divergent domains to be responsible for fat cell differentiation, while the conserved core of the protein performs a fundamental function in subcellular lipid storage (Tian et al., 2011; Cartwright and Goodman, 2012; Yang et al., 2013).

Indeed, seipin homologues are found in both plants and fungi, and the seipin gene in *Saccharomyces cerevisiae* is almost entirely composed of the conserved core domain (Szymanski et al., 2007). Two independent screens in yeast have reported a role for seipin in determining LD morphology (Szymanski et al., 2007; Fei et al., 2008). Although the yeast seipin homologue was termed *FLD1* due to apparently fewer LDs in an early fluorescence screen, the yeast seipin knockout phenotype is primarily marked by droplet heterogeneity. This includes clusters of small irregular droplets with electron-dense inclusions that are tangled in locally proliferated ER ("LD–ER tangles") that do not efficiently segregate during cytokinesis (Wolinski et al., 2011). Small abnormal droplets also accumulate in fibroblasts from seipin lipodystrophy patients, indicating that regulation of droplet morphology represents a conserved role for seipin in nonadipocytes (Szymanski et al., 2007). In addition to droplet clusters, supersized lipid droplets (SLDs) are also seen in the yeast seipin knockout, with volumes 30–50 times that of a typical wild-type droplet (Szymanski et al., 2007; Fei et al., 2008, 2011a; Wolinski et al., 2011). Supersized droplets in the absence of seipin are much more abundant during inositol starvation, a condition that suppresses PL synthesis (Henry et al., 2012), implying that droplet size in the seipin mutant is dependent on the ratio of PL to NL availability. Consistent with this, exogenous inositol reverses the supersized phenotype. (Fei et al., 2008, 2011a). Therefore droplet size and PL synthesis are apparently coupled in the absence of seipin; in contrast, droplet size is more independent of PL synthesis in the presence of this protein.

Seipin is a two-pass transmembrane protein in the ER, with short cytosolic N- and C-termini in yeast and larger, highly divergent cytosolic N- and C-terminal domains in metazoans (Windpassinger et al., 2004; Lundin et al., 2006; Szymanski et al., 2007). In mammalian cells, seipin may function through interaction with the sarco/endoplasmic reticulum Ca-ATPase (SERCA) pump (Bi et al., 2014). There is no SERCA orthologue in yeast, and we found that deletion of the probable ER calcium pump (Spf1p; Cronin et al., 2002) or pumps in the Golgi (Pmr1p) or vacuole (Pmc1p) does not phenocopy the seipin droplet phenotype (Supplemental Figure S1), suggesting that a disruption in ER–cytosolic calcium homeostasis is not causing the aberrant droplet phenotype in the absence of seipin in yeast. In yeast, however, seipin has been shown to associate with Ldb16, a protein with obscure function (Wang et al., 2014).

Within the ER, seipin concentrates in discrete puncta at LD–ER junctions (Szymanski et al., 2007; Fei et al., 2008). This localization and the effects of seipin deletion on LD morphology suggest that seipin is a facilitator or regulator of LD biogenesis. However, there has been no evidence that differentiates a role of seipin in droplet initiation versus downstream functions in droplet maintenance. To answer this question, we used a yeast system of inducible, synchronized de novo droplet formation. We report that seipin promotes LD formation under conditions in which NL synthesis is held constant. We also describe a new phenotype of the seipin-null strain, a high frequency of intranuclear droplets, indicating a role of seipin in vectorial droplet budding. Importantly, we describe an N-terminal deletion mutant with a slow rate of droplet initiation concomitant with large droplets but otherwise normal morphology and near normal vectorial budding. Our results indicate that facilitation of droplet initiation and control of droplet morphology and topology are separable functions of seipin (Cronin et al., 2002).

RESULTS

Seipin knockout drastically impedes de novo LD formation

To determine whether seipin plays a role in early stages of LD biogenesis, we used an *S. cerevisiae* strain in which the genes for all four NL synthetic enzymes (*DGA1*, *LRO1*, *ARE1*, and *ARE2*) were deleted ("4KO"). Unable to synthesize either triacylglycerol (TG) or steryl ester (SE), this strain lacks LDs (Oelkers et al., 2002). Initial experiments were conducted in which one of these genes, *DGA1*, was expressed under the galactose-inducible *GAL1-10* promoter on a low-copy plasmid, in either 4KO or 4KOfld1Δ (i.e., 4KO also lacking seipin) backgrounds. In glucose medium, *DGA1* expression was repressed and LDs were not observed. After derepression of *DGA1* by raffinose and induction by galactose, LD formation was observed by staining with the NL dye BODIPY 493/503, as expected (Supplemental Figure S2, A and B). The number of cells with fluorescent puncta began to increase at 3 h after induction, reaching 73% by 9 h (Supplemental Figure S2C). The number of puncta increased in the overall population as well as in individual cells that already contained them (Supplemental Figure S2D).

Deletion of seipin in the 4KO strain resulted in a small but significant decrease in the percent of cells generating BODIPY-staining material throughout induction, with greater differences at later time points (Supplemental Figure S2, A–C). Many of the fluorescent spots were significantly larger (Supplemental Figure S2E) and of heterogeneous shape with irregular borders, giving the impression of clusters of small droplets beyond the resolution limit of the microscope. We have therefore termed the BODIPY-staining material "fluorescent bodies" (FBs), as irregular clusters such as these cannot be quantified as individual LDs. All differences in FB number and morphology were rescued by expression of *FLD1* from a plasmid (unpublished data).

Similar results were obtained for cells inducibly expressing the steryl acyltransferase *ARE1* in the *4KO* background, although the *4KO-fld1Δ* defects were more modest in this system (Supplemental Figure S3), indicating that the role of seipin on droplet morphology is not limited to droplets composed of TG.

Careful analysis of FBs generated after 5 h of *DGA1* induction demonstrated aberrant morphology of FBs in the absence of seipin, consistent with phenotypes previously reported for *fld1Δ*. FBs were on average less intense with less distinct borders in the *4KOfld1Δ* strain and were accompanied by enhanced BODIPY staining of membranes (Supplemental Figure S4, A–D). Electron microscopy suggested that these dim, blurry FBs represent particularly large clusters of abundant, tiny LDs often associated with membrane (Supplemental Figure S4, E–H, J, and K). In addition, we noted droplets that appeared to be budding into the nucleus in 25% of cell thin sections (Supplemental Figure S4, I and L).

The de novo system identified a defect in LD formation in the absence of seipin and recapitulated several aspects of seipin-deficient LD morphology. However, the variance in the number and morphology of droplets among cells of each strain during induction was a significant concern in this plasmid-based system. A small fraction of cells (typically 5–8%) already displayed LDs at 0 h immediately before switching from raffinose into galactose medium, and 20–30% of *4KO* cells never developed LDs (Supplemental Figure S2C). These differences likely reflected variation in plasmid copy number and protein expression in the population. To achieve more uniform expression, we integrated the *GAL1-10* promoter at the endogenous *DGA1* locus in a strain lacking the other three acyltransferases, generating the strains *3KO($_{GAL}$DGA1)* and *3KO($_{GAL}$DGA1) fld1Δ*. A similar system has been reported by Jacquier and coworkers in the analysis of protein localization during de novo LD formation (Jacquier *et al.*, 2011). We also switched to a richer medium during induction to increase the rate of droplet formation.

Cells were analyzed at 0, 3, 6, and 9 h after the switch to galactose. Micrographs at 0 h revealed no BODIPY staining, except for a single droplet in a rare *3KO($_{GAL}$DGA1)* cell, while 82% of cells in this strain produced droplets after only 3 h; this number increased to 98% by 9 h after induction (Figure 1, A–C). By 9 h, cells typically contained approximately five droplets (Figure 1D).

Seipin-deficient cells produced a more striking LD biogenetic defect in the chromosomal system compared with expression of *DGA1* on a plasmid. FBs were detected in only 15% of *3KO($_{GAL}$DGA1) fld1Δ* cells by 3 h, and the number increased to only 27% of cells by 9 h (Figure 1, A and C). Those cells that did produce LDs displayed fewer FBs per cell (Figure 1D). This low-droplet phenotype was rescued by the addition of seipin encoded on a plasmid (Supplemental Figure S5). The phenotype was recapitulated in a strain in which *LRO1*, the other diacylglycerol (DG) acyltransferase, was substituted for *DGA1* in this system (unpublished data), indicating that the effect of seipin is not specifically linked to one of the TG-producing enzymes.

The slow formation of droplets in the *3KO($_{GAL}$DGA1) fld1Δ* strain could be caused by mistargeting of the acyltransferases. However, this appears not to be the case, at least for Dga1p. For assessment of targeting, the two DG acyltransferases were tagged in the genome with tdTomato (tdT). We found that tagged Dga1, which normally colocalizes with ER and droplets (Sorger and Daum, 2002), had the same behavior in the absence of seipin (Supplemental Figure S6, top rows). The targeting of tagged Lro1p was less clear. While we observed puncta that often associated with droplets in wild-type cells, as was recently reported (Wang and Lee, 2012), Lro1p-tdT in the *fld1Δ* strain, although still punctate, usually did not localize with droplets (Supplemental Figure S6, bottom rows). It is unclear whether the lower extent of droplet association of Lro1p in *fld1Δ* represents a targeting defect or simply reflects the fact that there are far fewer droplets on the ER with which to coincidently colocalize. While the effect of seipin on Lro1p localization needs further work to resolve, it is clear that the association of Dga1p with droplets does not require seipin, and therefore the LD biogenetic defects presented here are not a result of acyltransferase mistargeting.

As in the plasmid-based system, several morphological abnormalities were observed in the chromosomal system. While most *3KO($_{GAL}$DGA1)fld1Δ* cells lacked droplets throughout the experiment, they contained BODIPY-stained membrane rings, which were not observed in the parallel seipin-containing strain (Figure 1B, same microscope intensity settings). At later time points, the few FBs that appeared in the seipin-negative strain were large, irregularly shaped, and often diffuse, similar to the abnormal morphology observed in the *4KOfld1Δ* strain (Supplemental Figure 2, A and B). While the seipin-negative strain contained a relative dearth of droplets, the amounts of TG and DG acyltransferase activity were identical in both strains throughout the experiment (Figure 1, E and F), indicating that deficient TG synthesis is not responsible for the defect in *fld1Δ* LD formation. Overall both strains appeared healthy by morphology, and the growth rate during induction was identical (Figure 1G). Similar defects in de novo droplet formation were obtained in systems driving SE synthesis in *3KO($_{GAL}$ARE1)* strains (Supplemental Figure S7), confirming that the inhibitory effect of seipin on droplet formation is independent of NL type.

TG accumulates in membranes during LD formation in the absence of seipin

The normal levels of TG accumulation in the *3KO($_{GAL}$DGA1)fld1Δ* strain despite severely diminished LD formation suggested that TG was mislocalized within the cell. Indeed, the observation of BODIPY staining in a pattern suggestive of the ER membrane led us to hypothesize that TG is withheld in the ER as a result of impaired LD biogenesis in the absence of seipin.

To test the accumulation of TG in membranes biochemically, we harvested cells grown in galactose for 6 h. A membrane fraction was prepared and subjected to isopycnic centrifugation through a 1.0–1.9 M sucrose gradient, and fractions were then probed by immunoblotting for Dpm1p, an integral ER membrane marker (Orlean *et al.*, 1988). ER from the seipin-positive strain migrated to 1.47 M sucrose, while the bulk of membranes from the seipin-negative strain migrated lighter, to 1.33 M sucrose, consistent with the accumulation of NL in the ER in the absence of seipin (Figure 2A). Although a singular report indicated a partial localization of Dpm1p to droplets under some conditions (Takeda and Nakano, 2008), we failed to observe more than a trace (~1%) of Dpm1p in droplets in our system (Figure 2B; Erg6-DsRed and Sec63–green fluorescent protein [Sec63-GFP] were used as markers of droplets and ER, respectively). Mitochondria were also shifted to a lower density but to a smaller extent (Figure 2C), suggesting that the accumulated NL was not limited to the ER.

We also directly measured the amount of TG in purified LDs (from cells cultured in galactose medium for 6 h). While total cell TG was similar (Figure 2D), there was only 38% as much TG in droplets in the seipin-deletion strain (Figure 2E). Conversely, there was 46% more TG isolated from enriched ER membranes in this strain. These data show that TG accumulates in membranes in the absence of seipin, indicating that seipin plays a specific role in NL packaging.
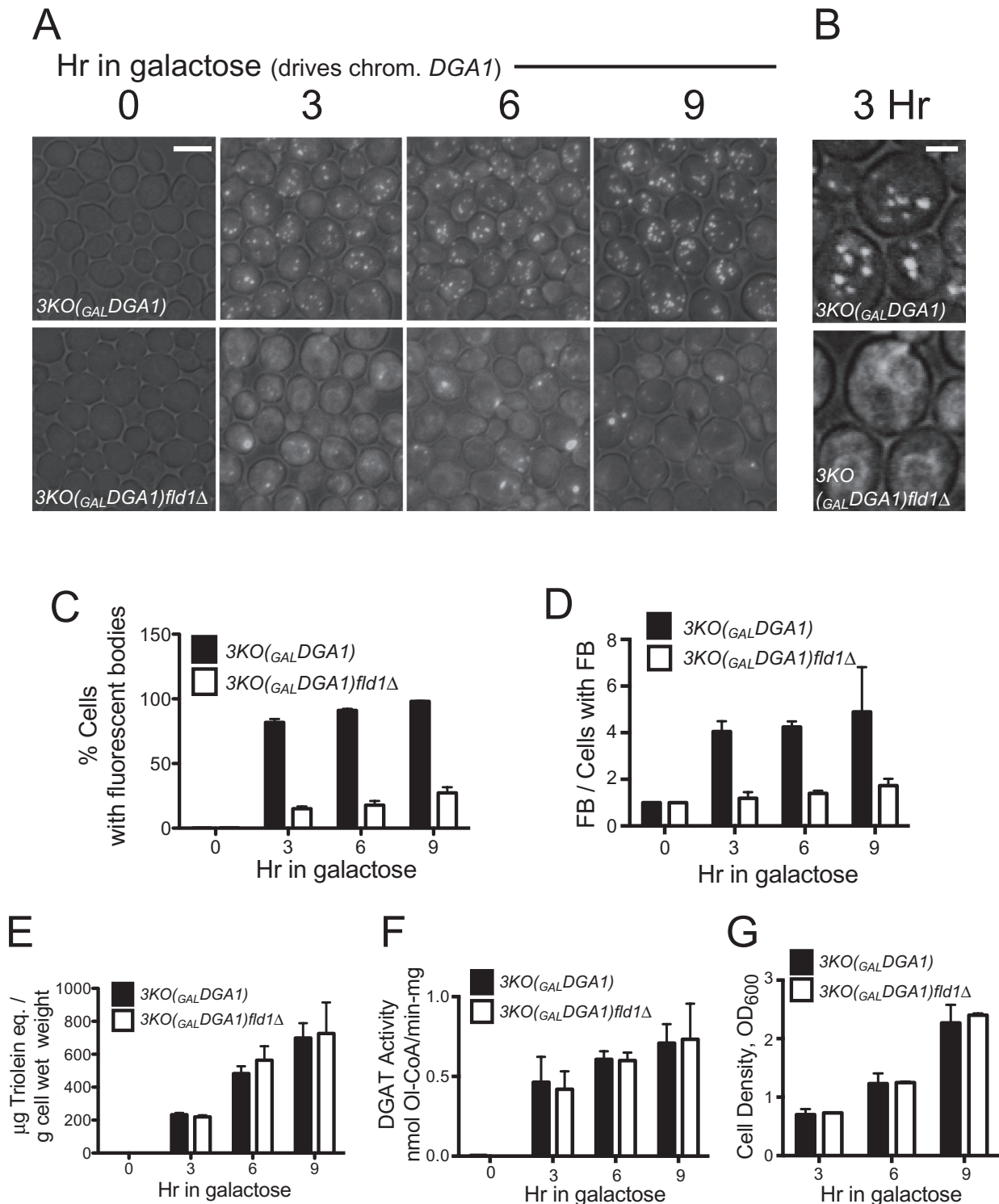
FIGURE 1: Seipin knockout drastically impedes de novo droplet formation. A galactose-inducible promoter was integrated into the genomic *DGA1* locus in a strain lacking the other three NL acyltransferases (*3KO($_{GAL}$DGA1)*) and in a strain with an additional seipin knockout (*3KO($_{GAL}$DGA1)fld1Δ*). Cells were introduced to rich galactose medium at $t = 0$ to induce droplet formation and stained with BODIPY at the indicated time points. (A) Representative fluorescence microscopy projection images at indicated time points after galactose induction, overlaid onto bright-field images. Scale bar: 5 μm. (B) Image of typical cells from each strain at 3 h. Scale bar: 2 μm. Intensity settings were kept constant between the two images to compare membrane brightness. (C) Percent of cells containing at least one FB. Error bars signify range from two experiments. (D) Number of distinct FBs per cells that have at least one FB. Error bars represent SDs from two experiments. (E) TG levels determined by TLC of lipid extracts from whole-cell lysates, normalized to cell pellet wet weight. Error bars represent range from 2 independent experiments. (F) TG synthesis activity of isolated membranes. Error bars signify SDs from two experiments. (G) Growth of cultures. Starting OD was 0.3. Error bars, SEM from two experiments, each performed in duplicate.
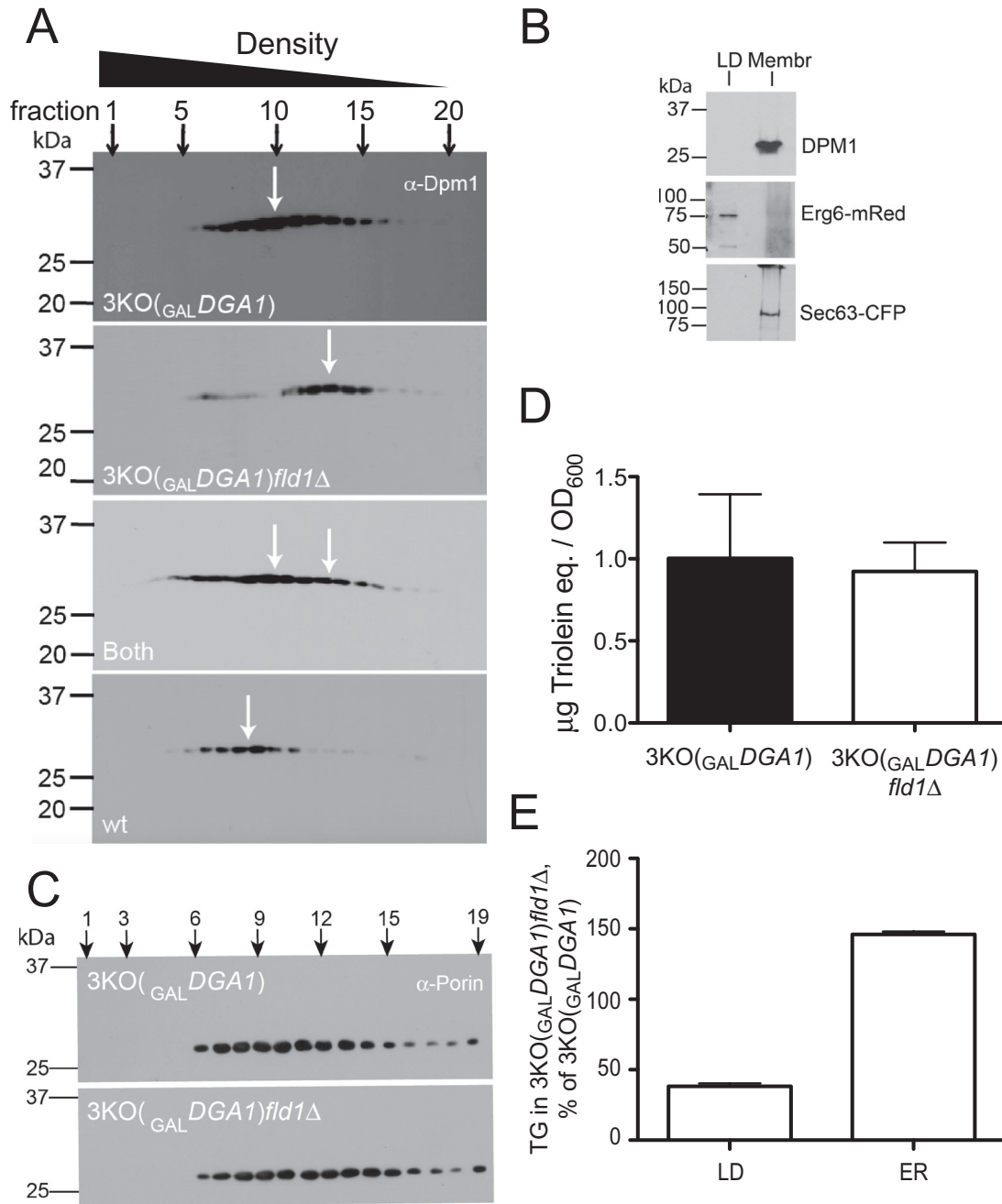
Seipin promotes lipid droplet biogenesis |

FIGURE 2: In the absence of seipin, TG accumulates in the ER during de novo LD formation. *3KO($_{GAL}$DGA1)* and *3KO($_{GAL}$DGA1)fld1Δ* cells were induced in rich galactose medium for 6 h, lysed, and fractionated. (A and C) Enriched ER membranes were centrifuged through a sucrose gradient, and fractions were blotted with α-Dpm1p (ER) or α-porin antibody. "Both" indicates a mixture of isolated membranes (4:1 *3KO($_{GAL}$DGA1)* to *3KO($_{GAL}$DGA1)fld1Δ* membranes by protein) from both strains; "wt" indicates the parental W303-1A strain. Representative blots for seipin from one of three independent experiments shown for *3KO($_{GAL}$DGA1)* and *3KO($_{GAL}$DGA1)fld1Δ* cells, and one of two independent experiments for porin. (B) Droplets and membranes from cells expressing Erg6-mRed and Sec63-GFP were separated and probed with α-Dpm1p or α-GFP; identical percents of LD and membrane fraction were analyzed. Parallel samples from cells expressing Erg6-DsRed were probed with α-DsRed. (Sec63-GFP interfered with the α-Erg6p signal.) Dpm1p is exclusively in the membrane fraction. (D) TG levels in the PNS fractions are compared in the strains indicated. (E) TG levels in the *3KO($_{GAL}$DGA1)* strain are compared with the *3KO($_{GAL}$DGA1)fld1Δ* strain in isolated droplets and enriched ER. The results of two experiments are shown in which organelles from the two strains were prepared in parallel. "100%" signifies the ratio of TG in the LD or ER fraction relative to TG in the PNS in the *3KO($_{GAL}$DGA1)* strain. Absolute values of TG (expressed as micrograms of trioleoyl glycerol equivalents) in the PNS and purified LDs are 697 and 88.9, respectively, in one experiment, and 263 and 52.4, respectively, for the other. Absolute values in the PNS and purified ER are 377 and 19.2, respectively, for one experiment, and 288 and 25.2, respectively, for the other. Comparison of these values with those from the *3KO($_{GAL}$DGA1)fld1Δ* strains reveals 36.5 and 40.2% (in the two experiments) as much TG in LDs from the seipin-minus strain, and 144 and 143% as much TAG in ER from the seipin-minus strain.
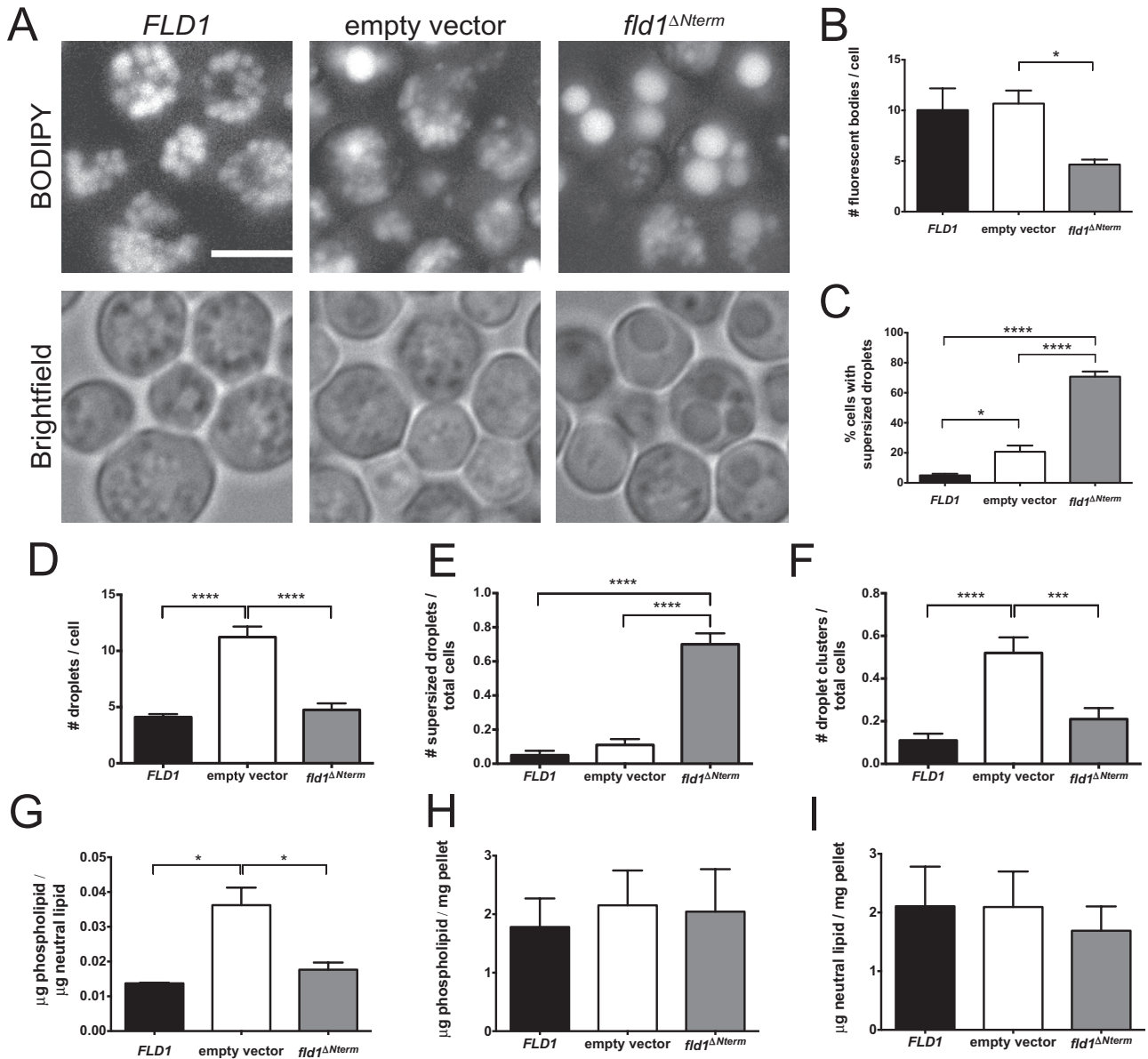
FIGURE 3: Deletion of 14 amino acids from the seipin N-terminus results in an SLD phenotype. Seipin knockout cells (*fld1Δ*) were complemented with plasmids overexpressing *FLD1*, *fld1ΔNterm*, or empty vector and cultured in rich oleate medium. (A) Representative bright-field or fluorescence microscopy projection images after staining with BODIPY to visualize LDs. Scale bar: 5 μm. (B) Number of FBs per total number of cells. (C) Percent of cells displaying one or more SLDs (defined as >1 μm diameter). For B and C, error bars represent SEMs from four independent experiments; for each, *n* = 100 cells from at least three fields. (D–F) Analysis of electron micrographs (sample images in Figure 4A); error bars represent SEMs from 100 cells. (D) Number of LDs per total number of cells. (E) Number of SLDs. (F) Number of LD clusters (defined as >5 adjacent droplets). (G) Phospholipid to NL ratios of isolated LD fractions, analyzed by TLC. (H) Phospholipid levels of whole-cell lysates by TLC, normalized to cell pellet wet weight. (I) Neutral lipid levels of whole-cell lysates as in H. (G–I) Error bars represent SEMs from four independent experiments. *, $p < 0.05$; **, $p < 0.01$; ***, $p < 0.001$; ****, $p < 0.0001$ by one-way analysis of variance (ANOVA) with correction for multiple comparisons.

Deletion of the seipin N-terminus results in a supersized LD phenotype

To dissect the role of seipin in LD formation, we screened a small panel of seipin-deletion mutants for defects in steady-state LD morphology (unpublished data). Most remarkable of these was a deletion of 14 amino acids (MKINVSRPLQFLQW), comprising the amino terminal domain that faces the cytosol and precedes the first membrane span. While the seipin-null strain is characterized by droplets of widely varying size, especially when cultured in medium containing

oleic acid (Szymanski *et al.*, 2007), cells expressing the N-terminal deletion mutant (*fld1ΔNterm*) from a plasmid in the null background resulted in a remarkable prominence of SLDs (Figure 3A). This is consistent with a recently reported phenotype of fewer, larger droplets for a 10–amino acid N-terminal deletion of seipin, which was not characterized further (Wang *et al.*, 2014). The *fld1ΔNterm* mutant produced fewer droplets per cell (Figure 3B) and more cells with SLDs (defined as LDs with >1-μm diameter by Yang; Fei *et al.*, 2011a; Figure 3C) than both wild-type and seipin knockout cells. The

overexpressed N-terminal deletion mutant protein both localized to the ER and formed high-molecular-weight complexes (Supplemental Figure S8), similar to wild-type. An SLD phenotype was also observed for endogenously expressed $fld1^{\Delta Nterm}$ integrated at the genomic seipin locus (Supplemental Figure S9A). Fluorescently tagged $fld1^{\Delta Nterm}$ forms several puncta similar to wild-type. Whereas wild-type seipin clearly localizes at or adjacent to the several droplets in cells, most puncta from $fld1^{\Delta Nterm}$ were dispersed in the cell, with at least one seipin spot associated with each of the few supersized droplets. (Supplemental Figure S9B).

The droplet phenotype from cells expressing $fld1^{\Delta Nterm}$ was compared with cells expressing $fld1^{\Delta Cterm}$ in which the cytoplasmically oriented final 12 amino acids at the carboxy terminus were deleted. As described previously with a 10–amino acid deletion at the C-terminus, chromosomal expression of $fld1^{\Delta Cterm}$ resulted in generally larger and fewer LDs (Supplemental Figure S10, top row). However, the size distribution was much more varied than the marked homogeneity observed among droplets from $fld1^{\Delta Nterm}$. The two seipin deletions at opposite ends of the protein produced opposite effects when they were overexpressed: while droplets remained very large for $fld1^{\Delta Nterm}$, overexpression of $fld1^{\Delta Cterm}$ resulted in an apparently wild-type phenotype of many small droplets (Supplemental Figure S10, bottom row). We conclude from these differences that the two termini of yeast seipin must have different functions. The function of the carboxy terminus was not further pursued in this study.

We further analyzed the supersized droplet phenotype of $fld1^{\Delta Nterm}$ from oleate-grown cells by electron microscopy (Figure 3, D–F; sample images are in Figure 4A), finding fewer droplets in $fld1^{\Delta Nterm}$ with an increased number of supersized droplets, consistent with the phenotype from fluorescence microscopy. Additionally, we detected a concomitant decrease in the prevalence of LD clusters (defined as at least five droplets adjacent to one another) compared with $fld1\Delta$ cells. This was consistent with a decrease in LD–ER tangles later observed by fluorescence microscopy in minimal medium (Figure 5, C and E). The N-terminal deletion therefore appears to display an extreme supersized phenotype but is otherwise normal in droplet morphology, without the droplet clustering or size heterogeneity of the knockout strain.

As described earlier, we often observed intranuclear droplets in the de novo system if seipin was absent, whereas this was never seen with seipin (Supplemental Figure S4, I and L). Similarly, intranuclear droplets were seen in most $fld1\Delta$ cells growing on oleic acid (Figure 4, A and B). Intranuclear droplets were also commonly seen by fluorescence microscopy (Figure 4, C and D). Such ectopic droplets were much scarcer in the $fld1^{\Delta Nterm}$, suggesting that the N-terminal domain may not be necessary for the vectorial budding of droplets promoted by seipin. We cannot rule out, however, that the decreased number of droplets in this strain could contribute to the relative scarcity of intranuclear droplets.

Measurement of the ratio of PL to NL in isolated droplets yielded results consistent with the observed morphology and surface/volume considerations. Thus the PL/NL ratio was elevated in droplets from the knockout strain, consistent with smaller droplets within ER tangles (Figure 3G). In contrast, we found that droplets isolated from $fld1^{\Delta Nterm}$ cells produced a strikingly lower PL/NL ratio than those isolated from $fld1\Delta$ cells. Unexpectedly, no difference in PL/NL ratio was detected between FLD1 and $fld1^{\Delta Nterm}$, despite the striking differences in LD size between these two strains. Predictions of PL/NL ratios based on a formula presented by Penno et al. (2013) and each strain's typical LD radius in rich oleate media (0.5 μm FLD1, 1.0 μm $fld1^{\Delta Nterm}$) were 1.2 and 0.56 mass%, respectively; difficulty in detecting small amounts of LD PL likely made this small difference indiscernible by our assay.

Importantly, droplet PL/NL composition differences occurred with no change in whole-cell PL or NL levels (Figure 3, H and I).

The N-terminal seipin-deletion phenotype is resistant to manipulation by inositol

Several yeast mutant strains, including $fld1\Delta$, have been characterized with SLD phenotypes that can be suppressed by PL precursors. Most are mutated in PL synthetic genes that are believed to generate SLDs as a result of poor PL availability, and these supersized droplets can be suppressed by supplementation of media with choline, ethanolamine, or inositol (Fei et al., 2011b). Unlike the PL synthetic mutants, however, SLDs in $fld1\Delta$ cells are only suppressed by inositol and actually worsened by ethanolamine.

Recently Wang and colleagues demonstrated that suppression of supersized droplets in $fld1\Delta$ by inositol resulted in a concomitant increase in the prevalence of droplet clusters, although they found no effect with ethanolamine treatment (Wang et al., 2014). We reproduced the effects of inositol in promoting LD–ER tangles (defined here as irregularly shaped FBs colocalizing with the ER marker cyan fluorescent protein ending with the tetrapeptidyl sequence HDEL [CFP-HDEL]) and suppressing SLDs in $fld1\Delta$ cells (Figure 5, A–C). While we could not detect an effect of ethanolamine in promoting SLDs, it did depress the formation of LD–ER tangles.

Strikingly, unlike those in $fld1\Delta$ cells, $fld1^{\Delta Nterm}$ LDs displayed no detectable response to supplementation with PL precursors in suppressing SLDs or promoting LD–ER tangles (Figure 5, A–C). The SLDs of $fld1^{\Delta Nterm}$ remained resistant even when inositol was applied at several-fold higher concentrations than that typically used for supplementation (Figure 5, D and E), and this relative resistance was reproduced in cells expressing $fld1^{\Delta Nterm}$ at endogenous levels (Supplemental Figure S9A). Because droplets were similarly unaffected by inositol in wild-type cells in this experiment, our data suggest that seipin with or without its amino terminus may protect droplets from changes in rates of PL synthesis.

N-terminal seipin deletion results in an initiation defect during de novo LD formation

After characterizing the effects of $fld1^{\Delta Nterm}$ on LD morphology and determining that the supersized phenotype was independent of inositol and its effect on PL synthesis, we then asked whether it could be explained by a defect in the rate of droplet initiation. We integrated $fld1^{\Delta Nterm}$ into the genomic seipin locus of the $3KO_{(GAL}DGA1)$ strain and observed LD formation after galactose induction as in Figure 1, with additional early time points at 1 and 2 h (Figure 6A). After 9 h, the "supersized" morphology of $fld1^{\Delta Nterm}$ was generally recapitulated, with the $fld1^{\Delta Nterm}$ droplet population displaying significantly larger sizes than FLD1 or $fld1\Delta$ (average area on projection image: FLD1, 55.02 pixels²; $fld1\Delta$, 80.43 pixels²; $fld1^{\Delta Nterm}$, 116.6 pixels²), obviously more spherical shape, and a size distribution that exhibited less skewness than $fld1\Delta$ (average skewness of area distributions: FLD1, 1.094; $fld1\Delta$, 2.189; $fld1^{\Delta Nterm}$, 1.406), indicating a more normally distributed droplet population than the knockout (Figure 6B).

Notably, at 2 h of galactose induction, $fld1^{\Delta Nterm}$ produced a significantly lower percentage of cells with at least one LD than FLD1 (Figure 6C), indicating a defect in the ability of $fld1^{\Delta Nterm}$ cells to initiate a droplet at early time points, similar to that of the $fld1\Delta$ strain. In cells that developed LDs, both $fld1\Delta$ and $fld1^{\Delta Nterm}$ produced fewer LDs per cell (Figure 6D). We decided to look more closely at the earliest stages of droplet formation by performing time-lapse microscopy on galactose-induced cells embedded in agar (Figure 6E and Supplemental Videos S1–S3). Cells were precultured at high
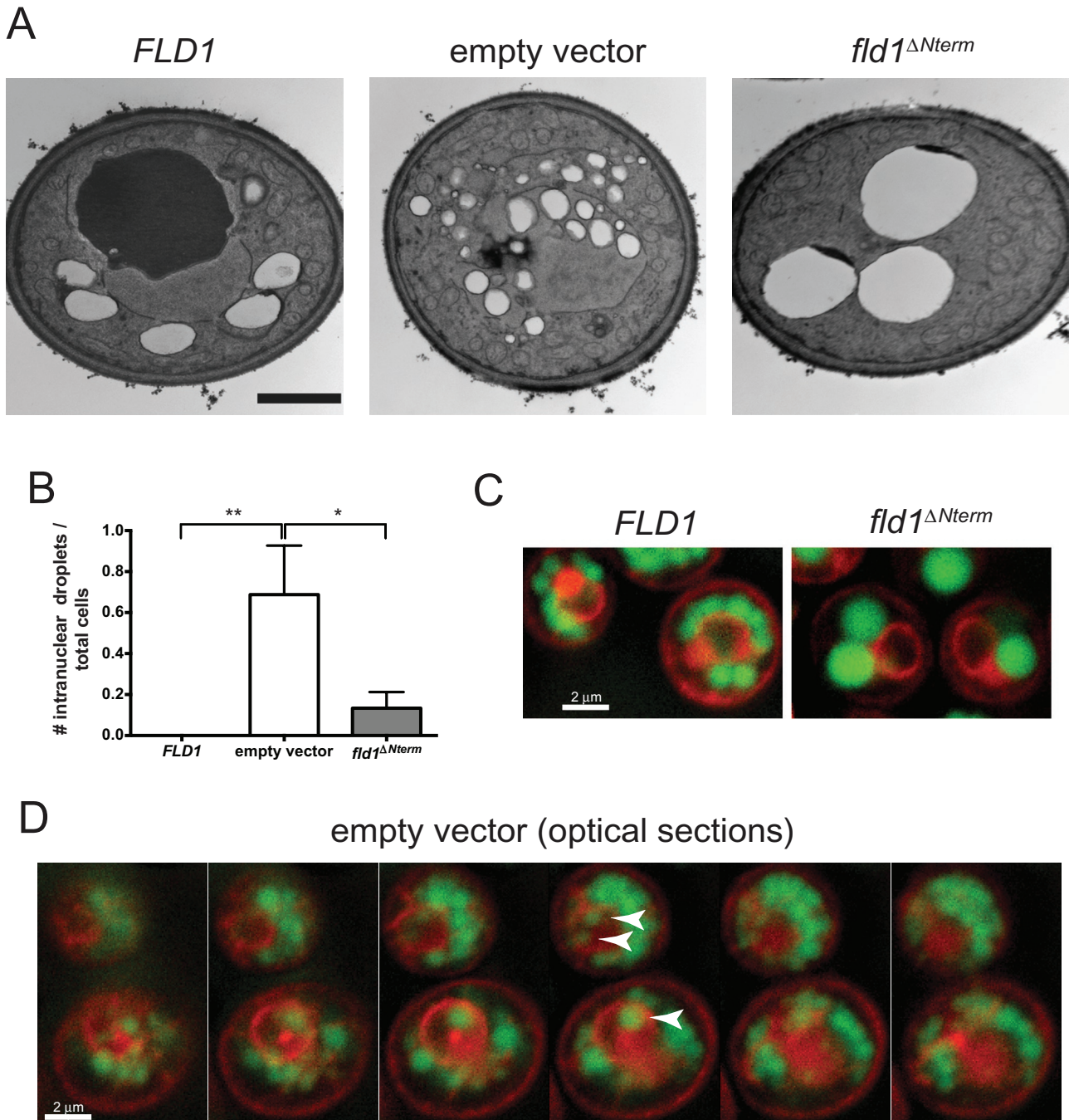
FIGURE 4: Nuclear LDs in the absence of seipin. Cells lines and culture conditions as in Figure 3. (A) Representative electron micrographs. Scale bar: 1 µm. (B) Number of intranuclear droplets (defined as within an observable, intact nuclear envelope). Error bars represent SEMs from ~30 cells sectioned at the level of a visible, intact nuclear envelope. (C and D) Cell lines also contained overexpressed CFP-HDEL to visualize the ER (false-colored red) and stained with BODIPY (green). (C) Fluorescence microscopy of fld1Δ cells containing *FLD1* or fld1[ΔNterm] as indicated. (D) Fluorescence microscopy of consecutive 0.3-µm z-sections of fld1Δ cells with empty vector. Arrowheads, intranuclear LDs.

density to prevent cell division during imaging. Development of droplets in the control *3KO(GALDGA1) FLD1* was less robust than in liquid culture, which might reflect the high density, low temperature on the stage (27–29°C), and/or suboptimal oxygenation. Nevertheless, while ~40% of *3KO(GALDGA1) FLD1* cells produced at least one droplet over the course of the experiment, very few fld1Δ or fld1[ΔNterm] cells (≤ 10%) produced a visible droplet during the experiment (Figure 5F).

Furthermore, we scored the time at which each cell developed its first LD and found that, while the majority of *FLD1* droplets were produced within 2 h of galactose induction, both fld1Δ and fld1[ΔNterm] displayed a severe deficit in the ability to produce a droplet at these early times (Figure 6G). Indeed, the lack of a peak at any time period suggests that the time to first droplet appearance is relatively stochastic in both mutant strains. We also analyzed the rate of droplet growth in these strains by measuring the change in the intensity of
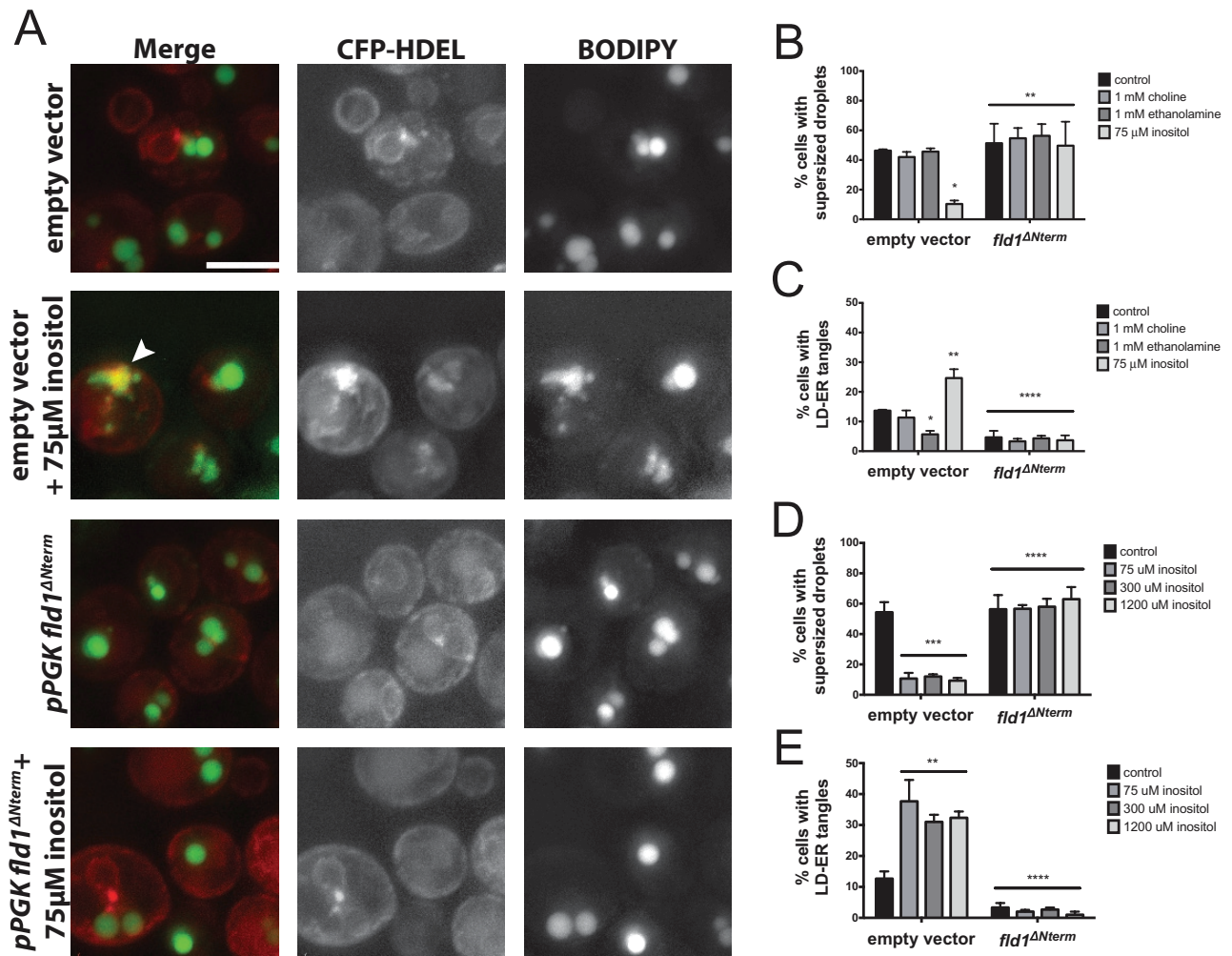
FIGURE 5: The N-terminal seipin-deletion phenotype is resistant to manipulation by inositol. Seipin knockout cells (*fld1Δ*) complemented with plasmids overexpressing empty vector, *FLD1*, or *fld1ΔNterm*, and the ER marker CFP-HDEL were grown in minimal glucose medium with or without the indicated PL precursor supplements. (A) Representative fluorescence microscopy projection images after staining with BODIPY. Scale bar: 5 µm. CFP-HDEL is false-colored red in the merged images. Arrowhead indicates an LD–ER tangle, defined as an irregular BODIPY body colocalized with a similarly shaped ER density. (B and D) Percent of cells displaying SLDs. (C and E) Percent of cells displaying LD–ER tangles. Error bars for B–E represent SEMs from three independent experiments; for each, $n = 100$ cells from at least three fields. *, $p < 0.05$; **, $p < 0.01$; ***, $p < 0.001$; ****, $p < 0.0001$ by two-way ANOVA with correction for multiple comparisons.

each LD over time. Surprisingly, we found that once a droplet appears, droplet growth is actually faster in both *fld1Δ* and *fld1ΔNterm* cells than in *FLD1*, indicating a suppression in LD initiation but not NL filling (Figure 6H), accounting for the larger droplet size. These data indicate that *fld1ΔNterm* has a defect in LD biogenesis similar to that of the *fld1Δ* strain, without the unusual morphological defects of *fld1Δ*. Our data indicate that the seipin N-terminus is important for droplet initiation but is dispensable for regulating droplet morphology other than size. Our data also suggest that seipin with or without its N-terminus controls PL entry into droplets and the vectorial budding of droplets toward the cytosol.

DISCUSSION

While morphological abnormalities of LDs in yeast seipin-null cells have been extensively characterized (Szymanski *et al.*, 2007; Fei *et al.*, 2008, 2011a; Wolinski *et al.*, 2011; Wang *et al.*, 2014), no study has yet determined whether seipin exerts these effects early in LD formation. We identified significant defects in de novo drop-

let formation in yeast cells lacking seipin, providing the first direct evidence that seipin functions in LD biogenesis. We found that these effects on LD formation were independent of effects on LD morphology, as an N-terminal seipin mutant displayed defects in LD initiation without producing aberrant droplet structures (other than their large size). Finally, we describe a novel phenotype of the seipin null cells in which droplets bud into the nucleus. We have therefore concluded that seipin exerts three distinct functions on the LD: 1) facilitating initiation of LD formation; 2) regulating the morphology and/or composition of LDs; and 3) channeling TG to bud directionally toward the cytosol (while retaining some attachment to the ER).

The effect of seipin on LD formation was independent of the source or amount of NL synthesized within the cell. While TG has been shown to increase in *fld1Δ* cells (Fei *et al.*, 2008), we saw no effects of seipin deletion on TG levels or TG synthesis rates in the *3KO(GALDGA1)* system. This is likely due to either the strong induction of NL synthesis from the *GAL1-10* promoter in our system or

differences in acute effects during early droplet formation compared with long-term effects in cells. We also observed a more profound effect on the formation of TAG droplets compared with SE droplets. Seipin may interact differently with these two classes of lipids, or there may be a partially redundant factor that promotes SE packaging. Another possibility is that unesterified sterol may increase in our *DGA1*-induction strains, due to knockout of the two steryl acyltransferases, and accumulation of free sterol within the ER could generate an additional barrier to LD formation by altering membrane properties. Regardless of the potential differences among these systems, we identified LD formation defects in every system tested, indicating that seipin acts broadly in the packaging of NL into LDs.

We found several lines of evidence demonstrating that, in the absence of seipin, LD biogenetic defects are accompanied by NL accumulation within the ER membrane. Biophysical studies and calculated predictions have indeed determined that NL can accumulate within a membrane bilayer up to 3–7 mass% before becoming unstable and "oiling out" (Gorrissen *et al.*, 1981, 1982; Hamilton and Small, 1981; Mackinnon *et al.*, 1992; King *et al.*, 1994; Khandelia *et al.*, 2010). We have therefore concluded that seipin functions in facilitating the release of NL from the ER into LDs and that, in the absence of this function, NL accumulates until it blebs stochastically from the ER.

Deleting the short cytosolic N-terminus of yeast seipin produced similar, though not as extreme, defects in LD formation, indicating this N-terminal region plays a key role in LD initiation. The mechanism by which seipin, specifically the N-terminus, might carry out this function remains to be determined. Many possibilities exist: seipin could act via direct channeling of NL, manipulation of localized ER membrane shape, or recruitment of enzymes for directed lipid synthesis; these are only a few of many potential mechanisms. Notably, phenotypes of seipin-null cells from yeast to humans bear a striking similarity to those deficient in lipin (Pah1p in yeast), a phosphatidic acid hydrolase that produces DG (Han *et al.*, 2006). Much like seipin, lipin is associated with lipodystrophy in mice, produces heterogeneous LD morphology with ER NL accumulation in yeast, and it or its activator localizes to the LD–ER junction (Klingenspor *et al.*, 1999; Reue *et al.*, 2000; Peterfy *et al.*, 2001; Adeyo *et al.*, 2011; Fei *et al.*, 2011a). The DG produced by yeast lipin was found to promote LD formation independent of its role as a TG precursor, and it has been suggested that DG could act as a cosurfactant with PLs in LD emulsion (Adeyo *et al.*, 2011; Thiam *et al.*, 2013). Additionally, a physical interaction between the human homologues of seipin and lipin was recently reported, although this appeared to be mediated by domains not conserved in yeast (Sim *et al.*, 2012, 2013). We therefore propose that a direct or indirect interaction between seipin and lipin is likely to be a strong candidate for the mechanism of seipin-facilitated LD formation.

Analysis of the seipin N-terminal deletion mutant also identified a role for seipin in the regulation of LD morphology, distinct from its role in LD biogenesis. Although *fld1*[ΔNterm] at least partially recapitulated the LD initiation defect of the seipin knockout, LDs in *fld1*[ΔNterm] were much more homogeneous in size and shape than those in *fld1*Δ. Indeed, the only apparent distinction between *fld1*[ΔNterm] and wild-type droplets was increased size and decreased number, likely caused by a limited number of droplets as a result of sluggish LD biogenesis. The lack of response of this mutant to manipulation by PL precursors provides a valuable clue to the mechanism of seipin action in promoting LD regularity. Because inositol and ethanolamine likely exert effects on *fld1*Δ LD morphology through PLs at the LD surface, we suggest that the bulk of the seipin protein (or some region other than the cytosolic N-terminus) may participate in the regulation or restriction of PL access to the LD surface. Seipin could act as a physical barrier to PL diffusion, an active transporter of certain PLs to the LD surface, a coordinator of new PL synthesis, or a determinant of local ER membrane shape. Further work is required to distinguish among these and other possibilities.

A recent report supports a role of seipin in promoting calcium trafficking from the cytosol into the ER lumen (Bi *et al.*, 2014). In mammalian cells, seipin was shown to physically interact with the SERCA pump and to provide stability to SERCA. The absence of seipin caused a reduction in pump activity, and loss of SERCA function phenocopied seipin-null cells. Our initial experiments in yeast found no effect of knockout of known calcium channels to LD morphology, however. Seipin may work through a yet-unidentified channel that did not appear in a BLAST search, or the function of yeast seipin may work through other mechanisms.

Our findings identify seipin as a key facilitator of LD biogenesis, thereby providing evidence that LDs do not spontaneously self-assemble. Indeed, LD biogenesis in the absence of seipin appears to occur stochastically, consistent with the "oiling out" or "spontaneous emulsion" of NL overwhelming the ER membrane. We therefore conclude that seipin acts as a catalyst in the facilitated emulsion of the LD. Furthermore, seipin plays an additional role in the regulation of homogeneous droplet morphology and content, and multiple lines of evidence demonstrate that seipin-deficient LDs are at least partially dysfunctional (Wolinski *et al.*, 2011; Chen *et al.*, 2012; Wang *et al.*, 2014). We propose that aberrant LDs produced in the absence of seipin do not represent true LD organelles; rather, they represent NL drops of unregulated composition that have coalesced by spontaneous emulsion. Our data therefore suggest that the lipodystrophy protein seipin is a required protein factor in the efficient and regulated biogenesis of the LD organelle.

MATERIALS AND METHODS
Materials
All chemicals were reagent grade. Fatty acid–free bovine serum albumin (BSA) was from Sigma-Aldrich (#A6003; St. Louis, MO). BODIPY 493/503 was purchased from Invitrogen (Carlsbad, CA) and stored at 1 mg/ml in dimethyl sulfoxide (DMSO). Anti-Dpm1p antibody was purchased from Abcam (5C5A7, ab 113686; Cambridge, MA), anti-DsRed from Clontech (Mountain View, CA), and anti-GFP from Roche (Indianapolis, IN). Neutral lipid standards were obtained from Nu-Chek (#TLC 18-5 C; Elysian, MN), 1,2-dioleoyl-*sn*-glycerol and PL standards (Soy PL mixture 690050C) were from Avanti Polar Lipids (Alabaster, AL). Oleoyl-1-^{14}C-CoA was from Perkin-Elmer Cetus (Waltham, MA). TLC plates were obtained from either Whatman/GE Healthcare (#4860-820; Pittsburgh, PA) or EMD Millipore (Silica Gel 60; Billerica, MA). Glass-bottom culture dishes were purchased from MatTek (#P36G-1.5-10-C; Ashland, MA).

Strains
Strains used in this study are listed in Supplemental Table S1. The BY4742 *fld1*Δ background strain used for overexpression of seipin mutants was obtained from the Yeast Knockout Collection (Open Biosystems). The acyltransferase knockout strains (*dga1*Δ*lro1*Δ, *are1*Δ*are2*Δ, and *dga1*Δ*lro1*Δ*are1*Δ*are2*Δ, termed "4KO"; Oelkers *et al.*, 2002) and the corresponding W303-1A wild-type were gifts of Steve Sturley (Columbia University). All the knockout and knock-in strains were generated by homologous recombination (Orr-Weaver *et al.*, 1981; Thomas and Rothstein, 1989). *FLD1* was knocked out of all strains (except those generated as controls for *fld1*[ΔNterm] knock-in) by substitution of the hygromycin phosphotransferase marker (*hph*) conferring resistance to the antibiotic, for the *FLD1* open reading
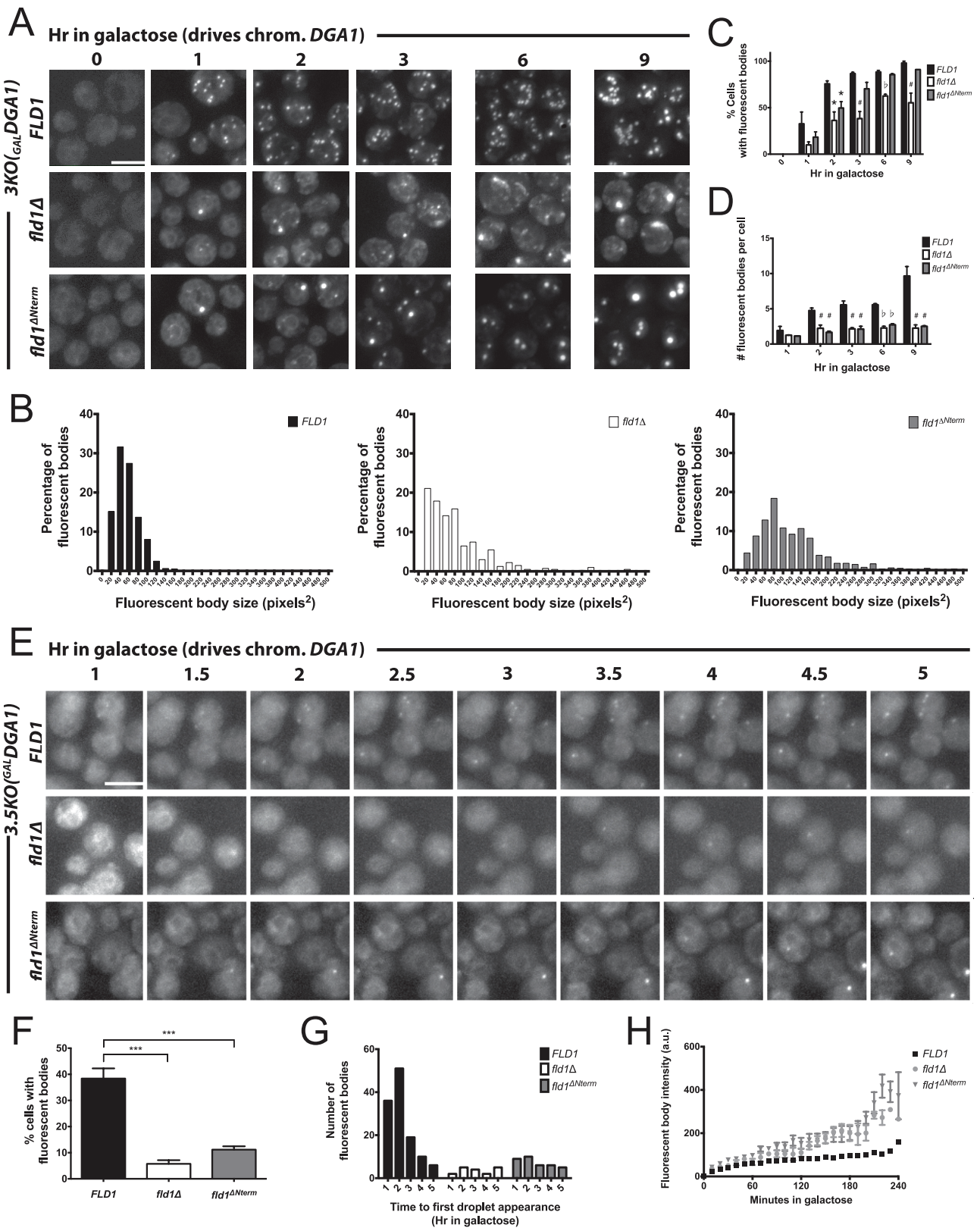
FIGURE 6: N-terminal seipin deletion results in an initiation defect during de novo LD formation. Genomic knock-ins were generated at the seipin locus in the *3KO(GALDGA1)* background for *FLD1, fld1Δ, and fld1ΔNterm*. Cells were switched from raffinose to galactose media at *t* = 0 to induce droplet formation and stained with BODIPY. (A) Representative fluorescence microscopy projection images at indicated time points after galactose induction. Scale bars: 5 μm. (B) Histograms of FB size, given as area in pixels on a maximum-intensity projection image. (C) Percent of cells containing at least one FB. (D) Number of distinct FBs per cells that have at least one. Error bars in C and D represent SEMs from three independent experiments, each *N* = 100 cells from at least three fields. *, *p* < 0.05; #, *p* < 0.01; ♭, *p* < 0.0001 by

frame (ORF). The *3KO(GALDGA1)* strain was generated from the *are1Δare2Δ* strain by substitution of *URA3* for *LRO1* ORF and then insertion of *TRP1* and the *GAL1-10* promoter cassette directly upstream of the *DGA1* ORF in the chromosome. In an analogous way, the *3KO(GALARE1)* strain was generated from the *dga1Δlro1Δ* strain by knockout of *ARE2* by substituting *HIS3* for the *ARE2* ORF and then inserting *TRP1* and the *GAL1-10* promoter cassette directly upstream of the *ARE1* ORF in the chromosome. Seipin-deletion mutant knock-ins were constructed in parallel with new corresponding wild-type and knockout strains to act as controls (either untagged or cloned with *tdTomato* just before the stop codon as indicated). These knock-ins were integrated in B74742 and *3KO(GALDGA1)* backgrounds by replacement of the *FLD1* ORF using the auxotrophic marker *ADE2*. Labeling of *DGA1* and *LRO1* with *tdTomato* was performed by introducing DNA encoding *tdTomato* with a 3Ala linker immediately downstream of the coding region, followed by the *PGK1* terminator (Szymanski *et al.*, 2007) and *URA3* for selecting transformants. Strains transformed with plasmids (see the following section and Supplemental Table S2) are indicated in the text or figure legends when appropriate (Thomas and Rothstein, 1989).

Plasmids

All plasmids used are listed and described in Supplemental Table S2; plasmids were transformed into background strains as described in the text or figure legends. Plasmids p^{GAL}*DGA1* and p^{GAL}*ARE1* were constructed for this study: the region between *GAL1* and *GAL10* ORFs (the *GAL* promoter) was cloned upstream of *DGA1* or *LRO1* for regulated expression of Dga1p and Are1p from plasmids (Sikorski and Hieter, 1989). The plasmid p^{PGK}*FLD1-mCherry* in the pRS412 vector (Brachmann *et al.*, 1998) was cloned from the corresponding plasmid in a pRS315 vector (Szymanski *et al.*, 2007) and used to transform the *4KOfld1Δ* and *3KOfld1Δ* strains to verify rescue to *4KO* and *3KO* phenotypes, respectively. The N-terminal deletion mutant *fld1^{ΔNterm}* was subcloned from *FLD1* into a p^{PGK} vector and then cloned into a p^{PGK}*mCherry* plasmid.

Growth conditions

All cultures were grown in liquid media in a shaking incubator at 30°C and 210 rpm. In each experiment, a colony from a plate was precultured for 18–48 h in minimal glucose medium before dilution in the indicated experimental media. Minimal medium refers to SC (synthetic complete) medium, consisting of Yeast Nitrogen Base (Bacto), 2% indicated sugar source (glucose for SCD, galactose for SCGal, or raffinose for SCR), and amino acid and base supplements (40 mg/l adenine, 20 mg/l arginine [HCl], 100 mg/l aspartic acid, 100 mg/l glutamic acid monosodium salt, 20 mg/l histidine, 60 mg/l leucine, 30 mg/l lycine [mono-HCl], 20 mg/l methionine, 50 mg/l phenylalanine, 375 mg/l serine, 200 mg/l threonine, 40 mg/l tryptophan, 30 mg/l tyrosine, 150 mg/l valine, 20 mg/l uracil, minus those required to maintain plasmids carrying auxotrophic markers). Rich galactose medium refers to YPGal, consisting of 10 g/l yeast extract (Bacto), 20 g/l peptone (Bacto), and 2% galactose. Rich oleate medium refers to YPO, consisting of 3 g/l yeast extract (Bacto), 16.9 g/l

peptone (Bacto), 0.5% potassium phosphate (5% stock buffered to pH 6.0), 0.2% Tween 80, and 0.1% oleate.

Cells grown in minimal glucose medium were diluted from the starter culture to a concentration of 0.1 OD$_{600}$/ml and grown to saturation unless otherwise indicated. Cells treated with oleate were additionally precultured in low glucose minimal medium (0.1% glucose) at 0.1 OD$_{600}$/ml and grown to saturation for 30 h before inoculation into rich oleate medium at a concentration of 1.0 OD$_{600}$/ml and incubation for 18–20 h. For galactose-induction experiments, cells were diluted from the starter glucose culture to 0.3 OD$_{600}$/ml in minimal raffinose medium (for derepression), grown for 18–24 h, and then diluted to 0.5 OD$_{600}$/ml in minimal (experiments shown in Figure 5 and Supplemental Figures S2 and S3) or rich galactose medium (Figures 1 and 2 and Supplemental Figures S5 and S6) to induce the acyltransferase. Samples were removed for analysis from raffinose cultures immediately before addition of galactose (*t* = 0) and from galactose cultures at remaining time points after induction. For time-lapse microscopy, the preculturing conditions were the same, with induction in rich galactose liquid medium for 30 min with BODIPY before processing for fluorescence microscopy (see the following section).

Fluorescence microscopy

Cells stained with BODIPY were pretreated to a final concentration of 0.2 μg/ml and incubated at 30°C and 210 rpm for 10–30 min immediately before collection by centrifugation at 3000 × *g* for 5 min. Two microliters was mounted onto a glass slide with an unsealed coverslip for imaging, except in time-lapse microscopy experiments, in which BODIPY-stained cells were resuspended in 10 μl liquid YP-Gal with 0.2 μg/ml BODIPY, and a 7.5-μl cell suspension was placed in the well of a 35-mm glass-bottom culture dish (MatTek #P35G-1.5-10-C) and mixed with 100 μl of melted YPGal with 0.2 μg/ml BODIPY and 1% agar at 42°C. Once solidified, cells in agar were overlaid with 5 ml YPGal with 0.2 μg/ml BODIPY.

All fluorescence images were acquired by a Sensican digital camera (Cooke) mounted on a Zeiss Axioplan 2E microscope using a 100×/1.3 NA oil objective. The following filter sets were used: FITC for GFP and BODIPY visualization (excitation, 490/25; emission, 528/38; 2-s exposure for GFP and 500-ms for BODIPY), CFP for CFP-HDEL visualization (excitation, 430/25; emission, 470/30; 2-s exposure), and CY3 for mCherry or tdTomato visualization (excitation, 555/28; emission, 617/23; 2-s exposure). Bright-field images were captured at 100-ms exposure. Samples for time-lapse microscopy were imaged on a Tempcontrol 37-2 heated stage (Zeiss) set for 37°C; measurements of liquid media indicated cells were heated to ~27–29°C. Ten to 20 z-sections in 0.5-μm steps were acquired and imaged in Slidebook (v. 4.1.0.3 or 5.5.2; Intelligent Imaging Innovations) and deconvolved using the nearest-neighbors method. Time-lapse images were manually refocused and captured every 10 min from 1 h after galactose induction to 5 h after induction. All images shown are maximal projections through the z-sections. Fluorescent bodies were manually counted and scored, except in Figure 5, C and D, where ImageJ was used to automatically quantify FBs after intensity thresholding.

---

one-way ANOVA with correction for multiple comparisons. (E) Time-lapse fluorescence microscopy of cells embedded into agar after 1 h of galactose induction in liquid culture at 27–29°C. Images taken in 10-min increments (see Supplemental Videos S1–S3); representative projections of 30-min increment montages are shown. Note that cells were precultured at high density to prevent division during imaging. (F) Percent of cells that displayed at least one FB over the course of the time lapse. Error bars represent SEMs from three independent experiments. ***, *p* < 0.001 by one-way ANOVA with correction for multiple comparisons. (G) Histogram of time to first appearance for each droplet. (H) Average intensity curves for FBs during the time lapse. Time 0 defined as the frame before first appearance of the droplet. Error bars represent SEMs from average droplet intensity values per time point over three independent experiments. Absolute intensity values are likely underestimated due to bleaching. Scale bars: 5 μm.

Seipin promotes lipid droplet biogenesis |

Electron microscopy

Cells were processed for electron microscopy as described previously (Wright, 2000; Binns *et al.*, 2006). Thin sections cut by the UT Southwestern Electron Microscope Facility were imaged on an FEI XL30 EXEM instrument.

Intracellular fractionation

Preparation of a postnuclear supernatant (PNS) and enriched ER fraction from yeast spheroplast extracts were performed according to our previous method (Binns *et al.*, 2010). For LD isolation or for comparison of composition of droplets with crude membranes, 900 μl of the PNS fraction was overlaid with 3 ml of 20 mM HEPES-KOH (pH 7.4), 100 mM KCl, 2 mM $MgCl_2$ 1 mM dithiothreitol (DTT), and protease inhibitors. Tubes were centrifuged at $120,000 \times g$ for 1 h at 4°C. The droplet cake was removed from the top by aspiration, and the pellet (membrane fraction) was resuspended in the PNS buffer. Equal percentages of fractions were loaded onto SDS gels or subjected to lipid extraction for analysis.

Detection of seipin oligomers

The oligomeric state of seipin and seipin$^{\Delta Nterm}$, expressed from plasmids p^{PGK}*FLD1-mCherry* and p^{PGK}*fld1$^{\Delta Nterm}$-mCherry*, respectively (see Supplemental Table S2), was determined after subjecting detergent extracts of ER-enriched membranes to velocity sedimentation on glycerol gradients according to our previous method (Binns *et al.*, 2010). Invisible pellets were suspended in 35% detergent-glycerol buffer and included in the analysis. Equal percentages of fractions were analyzed by immunoblots.

Analysis of lipids

For whole-cell lipids, 50 OD_{600} units were pipetted into a prechilled J14 tube (Beckman) and centrifuged $5000 \times g$ for 10 min at 4°C. Pellets were washed once with 50 ml cold sterile H_2O. Pellets were resuspended in 5 ml ice-cold H_2O and transferred to tared glass tubes on ice. Tubes were centrifuged at $3000 \times g$ for 5 min at 4°C. Supernatants were removed and recentrifuged to remove residual H_2O. Wet weights of pellets were determined. Pellets were resuspended in 400 μl of IP buffer (50 mM Tris-HCl, pH 8, 1 mM EDTA, 150 mM NaCl, 10% glycerol, 0.5 mM DTT) and transferred to 1.5-ml Eppendorf tubes. Acid-washed glass beads (0.5 g) were added, and tubes were vortexed at 4°C for 30 min. Samples were transferred back to the glass tubes, 2 ml isopropanol at 70°C was added for 30 min, and 1 ml chloroform was then added. Lipids were extracted overnight at 4°C. Further extractions and analysis of NLs by TLC were performed according to published methods (Chapman and Moore, 1993; Adeyo *et al.*, 2011). For analysis of PLs, plates were first developed for NLs as described, then air-dried for at least 1 h and further developed (in the same direction) with a solvent for separating PLs (Kuerschner *et al.*, 2008). For quantification, a dilution curve of standards was added to the TLC plate. Developed plates were charred several times, scanned, and quantified by densitometry in ImageJ. For lipids derived from subcellular fractions, the volume ratio of the first lipid extraction was adjusted to 450 μl aqueous sample:2 ml hot isopropanol:1 ml chloroform. Extractions then proceeded as before.

DG acyltransferase activity

ER-enriched membranes were isolated using our previous method (Binns *et al.*, 2010). Reactions were performed using a 55-μl reaction volume in glass tubes containing 150 mM HEPES-NaOH (pH 7.0), 2.5 mM $MgCl_2$, 0.1 mg/ml fatty acid–free BSA, 300 μM 1,2-dioleoyl-*sn*-glycerol, membranes at 0–20 μg protein (determined by Schaffner and Weissmann, 1973). Reactions were initiated by the addition of 0.05 μCi oleoyl-1-^{14}C-CoA diluted into cold oleoyl-CoA to yield a 91.6 μM final concentration in the reaction. After 20 min at 30°C with mild shaking (during which the reaction rate was linear), reactions were terminated by addition of 10 μl 10% SDS and placed immediately on ice. TG was added to 5 μg in each sample as a carrier, and the entire reaction was spotted onto a TLC plate. The plate was resolved in hexane:diethyl ether:acetic acid (80:20:1) for 55 min, allowed to dry, and then exposed to an imaging plate (FujiFilm, BAS-MP, 2040S) overnight. The TG spots, determined by comparison with the internal trioleoyl TG standard, were scraped off into liquid scintillant and counted. Activities for each reaction were determined by comparison with the specific activity of the oleoyl-CoA used to start the reaction, after subtracting the blank. Values were averaged from three protein concentrations in the assay.

REFERENCES

Adeyo O, Horn PJ, Lee S, Binns DD, Chandrahas A, Chapman KD, Goodman JM (2011). The yeast lipin orthologue Pah1p is important for biogenesis of lipid droplets. J Cell Biol 192, 1043–1055.

Agarwal AK, Garg A (2006). Genetic basis of lipodystrophies and management of metabolic complications. Annu Rev Med 57, 297–311.

Bi J, Wang W, Liu Z, Huang X, Jiang Q, Liu G, Wang Y, Huang X (2014). Seipin Promotes adipose tissue fat storage through the ER Ca^{2+}-ATPase SERCA. Cell Metab 19, 861–871.

Binns D, Januszewski T, Chen Y, Hill J, Markin VS, Zhao Y, Gilpin C, Chapman KD, Anderson RG, Goodman JM (2006). An intimate collaboration between peroxisomes and lipid bodies. J Cell Biol 173, 719–731.

Binns D, Lee S, Hilton CL, Jiang QX, Goodman JM (2010). Seipin is a discrete homooligomer. Biochemistry 49, 10747–10755.

Brachmann CB, Davies A, Cost GJ, Caputo E, Li J, Hieter P, Boeke JD (1998). Designer deletion strains derived from *Saccharomyces cerevisiae* S288C: a useful set of strains and plasmids for PCR-mediated gene disruption and other applications. Yeast 14, 115–132.

Cartwright BR, Goodman JM (2012). Seipin: from human disease to molecular mechanism. J Lipid Res 53, 1042–1055.

Chapman KD, Moore TS Jr (1993). N-acylphosphatidylethanolamine synthesis in plants: occurrence, molecular composition, and phospholipid origin. Arch Biochem Biophys 301, 21–33.

Chen W, Chang B, Saha P, Hartig SM, Li L, Reddy VT, Yang Y, Yechoor V, Mancini MA, Chan L (2012). Berardinelli-seip congenital lipodystrophy 2/seipin is a cell-autonomous regulator of lipolysis essential for adipocyte differentiation. Mol Cell Biol 32, 1099–1111.

Chen W, Yechoor VK, Chang BH, Li MV, March KL, Chan L (2009). The human lipodystrophy gene product Berardinelli-Seip congenital lipodystrophy 2/seipin plays a key role in adipocyte differentiation. Endocrinology 150, 4552–4561.

Cronin SR, Rao R, Hampton RY (2002). Cod1p/Spf1p is a P-type ATPase involved in ER function and Ca^{2+} homeostasis. J Cell Biol 157, 1017–1028.

Cui X, Wang Y, Tang Y, Liu Y, Zhao L, Deng J, Xu G, Peng X, Ju S, Liu G, Yang H (2011). Seipin ablation in mice results in severe generalized lipodystrophy. Hum Mol Genet 20, 3022–3030.

Fei W, Shui G, Gaeta B, Du X, Kuerschner L, Li P, Brown AJ, Wenk MR, Parton RG, Yang H (2008). Fld1p, a functional homologue of human seipin, regulates the size of lipid droplets in yeast. J Cell Biol 180, 473–482.

Fei W, Shui G, Zhang Y, Krahmer N, Ferguson C, Kapterian TS, Lin RC, Dawes IW, Brown AJ, Li P, *et al.* (2011a). A role for phosphatidic acid in the formation of "supersized" lipid droplets. PLoS Genet 7, e1002201.

Fei W, Zhong L, Ta MT, Shui G, Wenk MR, Yang H (2011b). The size and phospholipid composition of lipid droplets can influence their proteome. Biochem Biophys Res Commun 415, 455–462.

Fujimoto T, Parton RG (2011). Not just fat: the structure and function of the lipid droplet. Cold Spring Harb Perspect Biol 3, a004838.

Garg A (2004). Acquired and inherited lipodystrophies. N Engl J Med 350, 1220–1234.

Gong J, Sun Z, Wu L, Xu W, Schieber N, Xu D, Shui G, Yang H, Parton RG, Li P (2011). Fsp27 promotes lipid droplet growth by lipid exchange and transfer at lipid droplet contact sites. J Cell Biol 195, 953–963.

Goodman JM (2008). The gregarious lipid droplet. J Biol Chem 283, 28005–28009.

Goodman JM (2009). Demonstrated and inferred metabolism associated with cytosolic lipid droplets. J Lipid Res 50, 2148–2156.

Gorrissen H, Mackay AL, Wassall SR, Valic MI, Tulloch AP, Cushley RJ (1981). Deuterium magnetic resonance of selectively deuterated cholesteryl esters in dipalmitoyl phosphatidylcholine dispersions. Biochim Biophys Acta 644, 266–272.

Gorrissen H, Tulloch AP, Cushley RJ (1982). Deuterium magnetic resonance of triacylglycerols in phospholipid bilayers. Chem Phys Lipids 31, 245–255.

Granneman JG, Moore HP, Mottillo EP, Zhu Z, Zhou L (2011). Interactions of per-ilipin-5 (Plin5) with adipose triglyceride lipase. J Biol Chem 286, 5126–5135.

Gross DA, Zhan C, Silver DL (2011). Direct binding of triglyceride to fat storage-inducing transmembrane proteins 1 and 2 is important for lipid droplet formation. Proc Natl Acad Sci USA 108, 19581–19586.

Hamilton JA, Small DM (1981). Solubilization and localization of triolein in phosphatidylcholine bilayers: a 13C NMR study. Proc Natl Acad Sci USA 78, 6878–6882.

Han GS, Wu WI, Carman GM (2006). The Saccharomyces cerevisiae Lipin homolog is a Mg^{2+}-dependent phosphatidate phosphatase enzyme. J Biol Chem 281, 9210–9218.

Henry SA, Kohlwein SD, Carman GM (2012). Metabolism and regulation of glycerolipids in the yeast Saccharomyces cerevisiae. Genetics 190, 317–349.

Jacquier N, Choudhary V, Mari M, Toulmay A, Reggiori F, Schneiter R (2011). Lipid droplets are functionally connected to the endoplasmic reticulum in Saccharomyces cerevisiae. J Cell Sci 124, 2424–2437.

Khandelia H, Duelund L, Pakkanen KI, Ipsen JH (2010). Triglyceride blisters in lipid bilayers: implications for lipid droplet biogenesis and the mobile lipid signal in cancer cell membranes. PLoS One 5, e12811.

King NJ, Delikatny EJ, Holmes KT (1994). 1H magnetic resonance spectroscopy of primary human and murine cells of the myeloid lineage. Immunomethods 4, 188–198.

Klingenspor M, Xu P, Cohen RD, Welch C, Reue K (1999). Altered gene expression pattern in the fatty liver dystrophy mouse reveals impaired insulin-mediated cytoskeleton dynamics. J Biol Chem 274, 23078–23084.

Kuerschner L, Moessinger C, Thiele C (2008). Imaging of lipid biosynthesis: how a neutral lipid enters lipid droplets. Traffic 9, 338–352.

Kuhnlein RP (2011). The contribution of the Drosophila model to lipid droplet research. Prog Lipid Res 50, 348–356.

Le Lay S, Dugail I (2009). Connecting lipid droplet biology and the metabolic syndrome. Prog Lipid Res 48, 191–195.

Low KL, Shui G, Natter K, Yeo WK, Kohlwein SD, Dick T, Rao SP, Wenk MR (2010). Lipid droplet-associated proteins are involved in the biosynthesis and hydrolysis of triacylglycerol in Mycobacterium bovis bacillus Calmette-Guerin. J Biol Chem 285, 21662–21670.

Lundin C, Nordstrom R, Wagner K, Windpassinger C, Andersson H, von Heijne G, Nilsson I (2006). Membrane topology of the human seipin protein. FEBS Lett 580, 2281–2284.

Mackinnon WB, May GL, Mountford CE (1992). Esterified cholesterol and triglyceride are present in plasma membranes of Chinese hamster ovary cells. Eur J Biochem 205, 827–839.

Mak HY (2012). Lipid droplets as fat storage organelles in Caenorhabditis elegans: thematic review series: lipid droplet synthesis and metabolism: from yeast to man. J Lipid Res 53, 28–33.

Martin S, Parton RG (2006). Lipid droplets: a unified view of a dynamic organelle. Nat Rev Mol Cell Biol 7, 373–378.

Napier JA, Graham IA (2010). Tailoring plant lipid composition: designer oilseeds come of age. Curr Opin Plant Biol 13, 330–337.

Oelkers P, Cromley D, Padamsee M, Billheimer JT, Sturley SL (2002). The DGA1 gene determines a second triglyceride synthetic pathway in yeast. J Biol Chem 277, 8877–8881.

Orlean P, Albright C, Robbins PW (1988). Cloning and sequencing of the yeast gene for dolichol phosphate mannose synthase, an essential protein. J Biol Chem 263, 17499–17507.

Orr-Weaver TL, Szostak JW, Rothstein RJ (1981). Yeast transformation: a model system for the study of recombination. Proc Natl Acad Sci USA 78, 6354–6358.

Payne VA, Grimsey N, Tuthill A, Virtue S, Gray SL, Dalla Nora E, Semple RK, O'Rahilly S, Rochford JJ (2008). The human lipodystrophy gene BSCL2/seipin may be essential for normal adipocyte differentiation. Diabetes 57, 2055–2060.

Penno A, Hackenbroich G, Thiele C (2013). Phospholipids and lipid droplets. Biochim Biophys Acta 1831, 589–594.

Peterfy M, Phan J, Xu P, Reue K (2001). Lipodystrophy in the fld mouse results from mutation of a new gene encoding a nuclear protein, lipin. Nat Genet 27, 121–124.

Prieur X, Dollet L, Takahashi M, Nemani M, Pillot B, Le May C, Mounier C, Takigawa-Imamura H, Zelenika D, Matsuda F, et al. (2013). Thiazolidinediones partially reverse the metabolic disturbances observed in Bscl2/seipin-deficient mice. Diabetologia 56, 1813–1825.

Reue K, Xu P, Wang XP, Slavin BG (2000). Adipose tissue deficiency, glucose intolerance, and increased atherosclerosis result from mutation in the mouse fatty liver dystrophy (fld) gene. J Lipid Res 41, 1067–1076.

Schaffner W, Weissmann C (1973). A rapid, sensitive, and specific method for the determination of protein in dilute solution. Anal Biochem 56, 502–5014.

Sikorski RS, Hieter P (1989). A system of shuttle vectors and yeast host strains designed for efficient manipulation of DNA in Saccharomyces cerevisiae. Genetics 122, 19–27.

Sim MF, Dennis RJ, Aubry EM, Ramanathan N, Sembongi H, Saudek V, Ito D, O'Rahilly S, Siniossoglou S, Rochford JJ (2012). The human lipodystrophy protein seipin is an ER membrane adaptor for the adipogenic PA phosphatase lipin 1. Mol Metab 2, 38–46.

Sim MF, Talukder MM, Dennis RJ, O'Rahilly S, Edwardson JM, Rochford JJ (2013). Analysis of naturally occurring mutations in the human lipodystrophy protein seipin reveals multiple potential pathogenic mechanisms. Diabetologia 56, 2498–2506.

Skinner JR, Shew TM, Schwartz DM, Tzekov A, Lepus CM, Abumrad NA, Wolins NE (2009). Diacylglycerol enrichment of endoplasmic reticulum or lipid droplets recruits perilipin 3/TIP47 during lipid storage and mobilization. J Biol Chem 284, 30941–30948.

Sorger D, Daum G (2002). Synthesis of triacylglycerols by the acyl-coenzyme A:diacyl-glycerol acyltransferase Dga1p in lipid particles of the yeast Saccharomyces cerevisiae. J Bacteriol 184, 519–524.

Szymanski KM, Binns D, Bartz R, Grishin NV, Li WP, Agarwal AK, Garg A, Anderson RG, Goodman JM (2007). The lipodystrophy protein seipin is found at endoplasmic reticulum lipid droplet junctions and is important for droplet morphology. Proc Natl Acad Sci USA 104, 20890–20895.

Takeda Y, Nakano A (2008). In vitro formation of a novel type of membrane vesicles containing Dpm1p: putative transport vesicles for lipid droplets in budding yeast. J Biochem 143, 803–811.

Thiam AR, Farese RV Jr, Walther TC (2013). The biophysics and cell biology of lipid droplets. Nat Rev Mol Cell Biol 14, 775–786.

Thomas BJ, Rothstein R (1989). Elevated recombination rates in transcriptionally active DNA. Cell 56, 619–630.

Tian Y, Bi J, Shui G, Liu Z, Xiang Y, Liu Y, Wenk MR, Yang H, Huang X (2011). Tissue-autonomous function of Drosophila seipin in preventing ectopic lipid droplet formation. PLoS Genet 7, e1001364.

Wang CW, Lee SC (2012). The ubiquitin-like (UBX)-domain-containing protein Ubx2/Ubxd8 regulates lipid droplet homeostasis. J Cell Sci 125, 2930–2939.

Wang CW, Miao YH, Chang YS (2014). Control of lipid droplet size in budding yeast requires the collaboration between Fld1 and Ldb16. J Cell Sci 127, 1214–1228.

Wilfling F, Haas JT, Walther TC, Jr RV (2014). Lipid droplet biogenesis. Curr Opin Cell Biol 29, 39–45.

Wilfling F, Wang H, Haas JT, Krahmer N, Gould TJ, Uchida A, Cheng JX, Graham M, Christiano R, Frohlich F, et al. (2013). Triacylglycerol synthesis enzymes mediate lipid droplet growth by relocalizing from the ER to lipid droplets. Dev Cell 24, 384–399.

Windpassinger C, Auer-Grumbach M, Irobi J, Patel H, Petek E, Horl G, Malli R, Reed JA, Dierick I, Verpoorten N, et al. (2004). Heterozygous missense mutations in BSCL2 are associated with distal hereditary motor neuropathy and Silver syndrome. Nat Genet 36, 271–276.

Wolinski H, Kolb D, Hermann S, Koning RI, Kohlwein SD (2011). A role for seipin in lipid droplet dynamics and inheritance in yeast. J Cell Sci 124, 3894–3904.

Wright R (2000). Transmission electron microscopy of yeast. Microsc Res Tech 51, 496–510.

Yang L, Ding Y, Chen Y, Zhang S, Huo C, Wang Y, Yu J, Zhang P, Na H, Zhang H, et al. (2012). The proteomics of lipid droplets: structure, dynamics, and functions of the organelle conserved from bacteria to humans. J Lipid Res 53, 1245–1253.

Yang W, Thein S, Guo X, Xu F, Venkatesh B, Sugii S, Radda GK, Han W (2013). Seipin differentially regulates lipogenesis and adipogenesis through a conserved core sequence and an evolutionarily acquired C-terminus. Biochem J 452, 37–44.

Zanghellini J, Wodlei F, von Grunberg HH (2010). Phospholipid demixing and the birth of a lipid droplet. J Theor Biol 264, 952–961.